




Direct ink writing of TiC–316L metal matrix composites with an epoxy resin–absolute ethanol system

Tao Lin* , Liu-Ping Jin, Jia-Yun Yuan, Hui-Ping Shao, Fu-Cheng Yu, Wen-Yuan Li, Xin-Bo He, Xin Deng

Received: 16 February 2020 / Revised: 7 May 2020 / Accepted: 29 September 2020 / Published online: 22 October 2020
© GRINM Bohan (Beijing) Publishing Co., Ltd 2020

Abstract TiC–316L metal matrix composites were successfully printed with an epoxy resin–absolute ethanol system by direct ink writing (DIW) process in this study. Microstructure and fracture morphology of the samples were observed by a scanning electron microscope (SEM). Also, the relative density, hardness and transverse rupture strength (TRS) of the sintered samples were tested. The results show that the samples prepared with a new epoxy resin–absolute ethanol system by the DIW process have high solid content of printing slurry, good surface roughness, high relative density and high strength. The solid content of the slurry suitable for DIW was 60 vol%, and the internal diameter of the nozzle was set to 0.4 mm, the printing speed was set to 30 mm·s⁻¹, and the layer height was set to 0.36 mm. For the sample with 35 wt% TiC–316L, the relative density, hardness and TRS of the sintered sample can reach 99.3%, HRA 79.5 and 1438 MPa, respectively.

Keywords DIW; MMCs; Epoxy resin; TiC; 316L

T. Lin*, L.-P. Jin, J.-Y. Yuan, H.-P. Shao, W.-Y. Li, X.-B. He
Institute for Advanced Materials and Technology, University of
Science and Technology Beijing, Beijing 100083, China
e-mail: lintao@ustb.edu.cn

F.-C. Yu
School of Material Science and Engineering, Lanzhou
University of Technology, Lanzhou 730050, China

X. Deng
Jihua Laboratory, Chengye Mansion, Foshan 528299, China

X. Deng
School of Electromechanical Engineering, Guangdong
University of Technology, Guangzhou 510006, China

1 Introduction

Metal matrix composites (MMCs) are used in a broad variety of industries, including chemical processing, aerospace, automotive, pulp and paper, oil and gas, etc., due to the high wear resistance [1–3]. In recent years, there have been increasing demands among various industries for MMCs due to their high strength and stiffness and their outstanding wear resistance [4–7]. MMCs which use TiC as hard phase have the following advantages [8, 9]. (1) TiC has a moderate cost because of rich reserves of its raw material and the simple process to prepare it; (2) With the addition of MMCs of TiC particles, the grain growth of the matrix is reduced and the strength is increased; (3) TiC particles improve the hardness, thermal stability and oxidation resistance of the composite material; (4) Carbon content of the composite can be adjusted in a large range so that composition of the composite can be flexibly designed. (5) Density of TiC (4.90 g·cm⁻³) is only one-third of that of the WC so that the composite has the advantages when utilized as wear resistant materials carrying vehicles and aerospace vehicles.

MMCs are typically prepared by methods such as casting, powder metallurgy because they are hard to be machined. However, the major problem associated with these conventional processing routes comes from molds [10], since preparation of molds is complicated and time-consuming. Therefore, there is a need for near net formation without molds.

Three-dimensional (3D) printing, also known as additive manufacturing, is currently the most popular near-net forming process without molds. As for common 3D printing methods, laser selective sintering (SLS) and laser selective melting (SLM) are the representative ones for manufacturing metal materials. Complex shape parts are

prepared by repeatedly stacking the layers of particles and directly sintering or melting particles in the selected area by laser. In recent years, 3D printing processes with laser have been used to prepare some kinds of MMCs. Betts et al. [11] used direct laser deposition to prepare Al_2O_3 -316, WC-316 and Cr_3C_2 -316 MMCs, in which wear resistance was improved by 260 times and corrosion resistance by one time with the addition of WC particles. The addition of Cr_3C_2 improved the wear resistance by 88 times and the corrosion resistance by 2–3 times. Song et al. [12] used SLM to prepare TiC–FeAl MMCs. Compared with FeAl products, TiC–FeAl composites have higher hardness, elastic modulus and better wear resistance. Amorim et al. [13] used SLS to prepare TiB_2 -CuNi MMCs, which can be used to directly produce electrical discharge machining (EDM) electrodes. Prabhakar et al. used direct laser metal sintering process to prepare SiC–Fe MMCs, and evaluated the density, microstructure and micro-hardness of laser-sintered SiC–Fe samples [14]. Wang et al. [15] used SLS to prepare WC–Co composite materials, and realized using commercially available powders to produce hard alloy parts with high mechanical properties and high wear resistance. Yao et al. [16] used SLM to prepare TiC–IN718 composites. IN718 is a nickel-based austenitic super-alloy. The nano-TiC as a reinforcing phase acted to refine grain and pinch grain boundary dislocations, thereby increasing the tensile strength of the TiC–IN718 composite. The equipment for laser 3D printing process is more complex and expensive and its requirements for powders are also strictly in terms of particle size, particle size distribution and shape.

DIW is a versatile additive manufacturing process which can be used to prepare ceramics, composites and hydrogels. Recently, researchers have applied three-dimensional printing (3DP) to prepare layered porous ceramics [17], chitosan–silica composites [18], cellulose nanocrystals [19], magnetic materials [20] and other materials.

In our previous research [21], a 3D gel-printing (3DGP) process based on hydroxyethyl methacrylate (HEMA) gel system in which the solvent was toluene was proposed. This is also a kind of DIW process. The 316L stainless steel gears and ceramic parts were successfully prepared with the HEMA system by 3DGP [21–23]. In this process, free radical polymerization of organics in gel system was used to form polymer network to fix particles and realize in situ curing. With advantages such as the simple device structure and higher printing rate, 3DGP process can be used in a wider range of materials, such as ceramics and ceramic matrix composites, metals and MMCs.

The HEMA system has a higher toxicity in consideration of its composition: methacrylate-2-hydroxy ethyl, toluene N,N,N,N-tetramethylethylenediamine, benzoyl

peroxide. Epoxy resin has the advantages of strong adhesion, easy curing, low shrinkage after curing and low toxicity. The cured epoxy resin has certain mechanical properties. A small amount of epoxy resin can be dissolved in absolute ethanol [24, 25].

In this study, TiC–316L MMCs were successfully prepared by the DIW process with an epoxy resin–absolute ethanol system. The epoxy resin–absolute ethanol system is lowly toxic and harmless compared with HEMA system. Also, the solid volume content of slurry could be increased to more than 60 vol%. Therefore, the epoxy resin–absolute ethanol system is a relatively better choice for preparing MMCs.

2 Experimental

2.1 Materials

TiC powder (Hunan Metallurgy Materials Institute) and 316L stainless steel powder (Fujian Tianzhi Alloy Materials Co., Ltd.) used as raw powder in this study have an average particle size of 6.43 and 10.45 μm , respectively (tested by the laser diffraction method).

Figure 1 shows the particle size distribution and the morphology of TiC powder and 316L stainless steel powder, respectively. As shown in Fig. 1a, the TiC powder has irregular shapes and there are a few bigger particles. As shown in Fig. 1b, most of the particles are nearly spherical in the 316L powder. Compared with that of TiC powder, the particle size distribution range of the 316L powder is wider, and there are a few bigger particles at the same time. An epoxy resin–absolute ethanol system was used in this study as an organic binder, in which the organic solvent was absolute ethanol and the dispersant was oleic acid produced by Sinopharm Chemical Reagent Co. Ltd. Epoxy resin and its curing agent are also produced by Sinopharm Chemical Reagent Co., Ltd. They are all the analytical pure.

2.2 Preparation of printing slurry

First, TiC powder and 316L stainless steel powder were mixed proportionally, and the content of TiC powder in the mixed powder is 10 wt%, 35 wt% and 50 wt%, respectively.

In order to ensure the uniformity of the powders, the mixture of TiC and 316L powders was milled by a planetary ball mill with cemented carbide balls and ethanol for 10 h. The mass ratio of the balls and powder was 4:1, and the speed of the ball mill was 220 $\text{r}\cdot\text{min}^{-1}$. After drying and sieving, the morphology of the mixture was observed with scanning electron microscope (SEM)

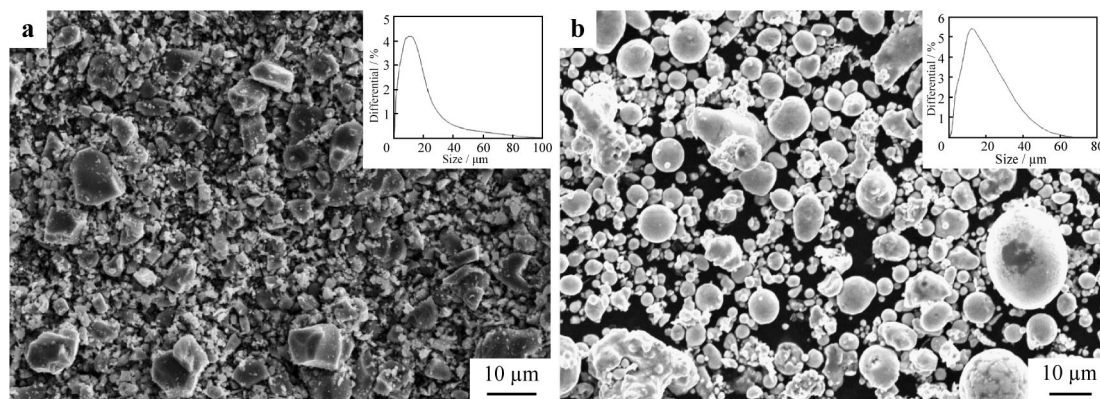


Fig. 1 SEM images and particle size distribution (insets) of raw powders: **a** TiC powder and **b** 316L stainless steel powder

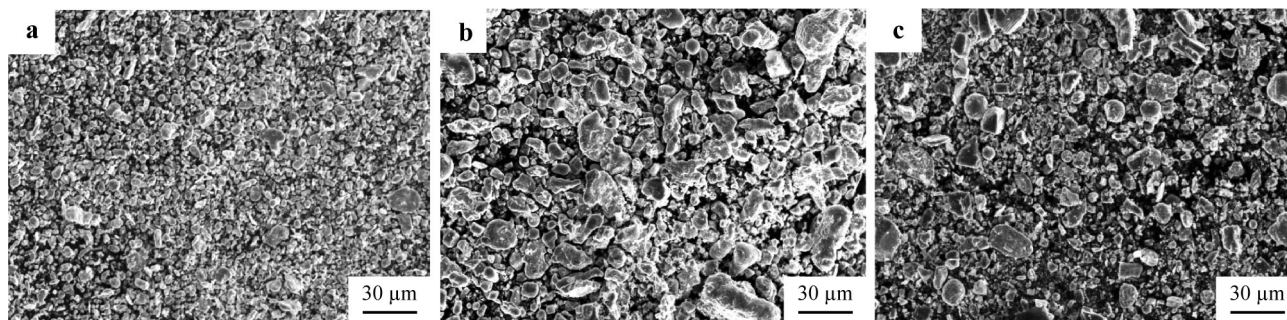


Fig. 2 SEM images of mixed TiC–316L powders with different TiC contents: **a** 10 wt%, **b** 35 wt% and **c** 50 wt%

as shown in Fig. 2. It can be seen that these two powders were mixed with each other and 316L particles with the nearly spherical shape and TiC particles with the polygonal shape could not be distinguished from each other by their shape.

The slurry used in this study was prepared as follows: the organic solvent absolute ethyl alcohol, the epoxy resin and the curing agent were mixed according to a certain proportion. Then, the mixture was stirred to obtain the premixed solution with addition of the dispersant oleic acid.

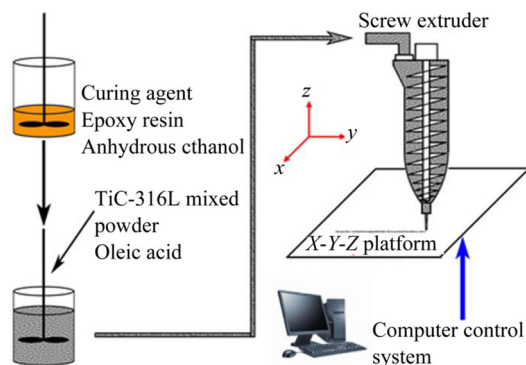


Fig. 3 Schematic diagram of DIW process

2.3 DIW process

As shown in Fig. 3, the slurry was used to prepare TiC–316L composite samples via a DIW device.

Figure 3 shows the schematic diagram of the DIW process. The device includes three main components: a screw extruder (3GN-25K, Taili Motor Co. Ltd.), an X–Y–Z platform and a computer control system. The diameter of the screw is 15 mm. The screw extruder was used to ensure the continuous and smooth extrusion of the slurry. The computer control system was used to control the movement of the X–Y–Z platform and the screw extruder, thereby realizing the layer-by-layer printing of 3D samples.

Curing of the slurry with the epoxy-anhydrous ethanol system occurs during printing of the sample and after printing is completed. The first curing process was performed slowly after the preparation of the slurry was completed. The curing time is much longer than the time that the slurry was put in the printing device. When the slurry was loaded into the printing device, the curing rate of the process is also very slow. The slurry has a low viscosity at the nozzle due to shear thinning effect which is beneficial for the slurry to be extruded out of the nozzle. The shear force disappears after extrusion, the viscosity and viscoelasticity of the slurry recover rapidly, and the

slurry can keep at the printing site in situ. At this time, the printed slurry has a low degree of curing, and has the binding ability and deformation ability. With the volatilization of absolute ethanol in the slurry, the polymerization speed is increased under the action of curing agent, the strength of green sample is improved rapidly, and the binding ability and deformation ability decrease slowly. After printing, the sample needs to be cured for about 24 h, and the absolute ethanol volatilizes further at room temperature. Under the action of epoxy resin curing, the strength of the green body increases gradually and eventually reaches at a value for further operating. The polymerization speed of the slurry with the epoxy resin–absolute ethanol system in the printing device is very slow and has little effect on the extrusion of the slurry, so it is not able to cause the problems for the printing device such as nozzle blockage.

The key printing parameters affecting the sample quality are nozzle size, printing speed and layer height. These printing parameters have also been studied in this study.

2.4 Sintering of samples

After the green samples were dried completely, the samples were degreased and sintered. A powder metallurgy vacuum sintering furnace (GZL-45, Zhuzhou Risheng Powder Metallurgy Equipment Manufacturing Co. Ltd.) with the combination of degreasing and sintering was used to degrease and sinter the samples and the samples cooled in the furnace after sintering. The printed samples were degreased at 450 °C for 2 h [26] and then sintered at 1390, 1450 and 1480 °C, respectively, with the TiC content of 10 wt%, 35 wt% and 50 wt% for 2 h.

2.5 Characterization

The particle size distribution was tested by a laser particle size analyzer (BT-9300S, Dandong Better Co. Ltd., China). The microstructures of the powder, green samples and sintered samples were characterized by a scanning electron microscope (SEM, ZEISS EVO®18, Carl Zeiss NTS, and Germany). The viscosity of the slurry was tested according to ASTM D4016-14 standard. The densities of the sintered composites were tested according to ASTM B311-13 standard. The hardness values of sintered composites were tested according to ASTM E18-16 standard. The TRS of sintered composites were tested according to ASTM B528-16 standard. The surface roughness values of samples were tested by a laser confocal microscope. Measured with a Vernier caliper, the size tolerance of the green body is 0.2 mm relative to its computer-aided design (CAD) mode.

3 Results and discussion

3.1 Rheological properties of slurry

Figure 4 shows the rheological behavior of the epoxy resin–absolute ethanol TiC–316L slurry. As shown in Fig. 4, the viscosity of the epoxy resin–absolute ethanol slurry decreases greatly from high shear rate to low shear rate, the slurry has a pseudo-plastic behavior. This means that the slurry has a low viscosity at the nozzle due to shear thinning effect which is beneficial for the slurry to be extruded out of the nozzle. The shear force disappears after the slurry is extruded out of the nozzle; thus, the viscosity and viscoelasticity of the slurry recover rapidly, and the slurry can keep at the printing site in situ. In addition, the viscosity changes caused by changing composition and solid content have little effect on printing of the slurry. As shown in Fig. 4, when the solid content is 50 vol% and 55 vol%, the resin was not only coated with powder, but also existed redundantly; therefore, the viscosity of the system is low. But when the solid content of the powder reaches 60 vol%, the resin completely covered the powder with almost no residue. At this time, the viscosity of the slurry system is relatively large. If the solid content exceeds 60 vol%, the resin cannot completely cover the powder at this time, and the system has almost no fluidity and cannot be printed. The maximum solid content suitable for printing is 60 vol%. This is a higher level of the solid content for the DIW process, which will be benefit for enhancing the densification and avoiding the deformation during sintering of the printed samples.

3.2 Homogeneity of slurry and samples

To ensure the slurry homogeneity, oleic acid was added as a dispersant to improve the dispersion and suspension of the particles in the mixed organic solution. If no oleic acid was added, the solid content in the slurry was no more than 40 vol% and the solid particles agglomerated and were hardly to disperse homogeneously. To prevent particles from settling during printing, there is a blade for stirring in the slurry can, and the screw of the screw extruder also has the role of stirring. TiC and 316L particles are homogeneously presented in the printed sample as shown in Fig. 5a. Furthermore, TiC particles are homogeneously dispersed in the 316L matrix of sintered body, as shown in Fig. 5b. These results illustrate that the TiC particles and 316L particles were mixed with each other homogeneously in the printed green sample.

The 316L metal powder used herein with a spherical shape and a particle size of 10 μm was prepared by gas-atomization for metal injection molding (MIM) applications, and the TiC ceramic powder generally has a

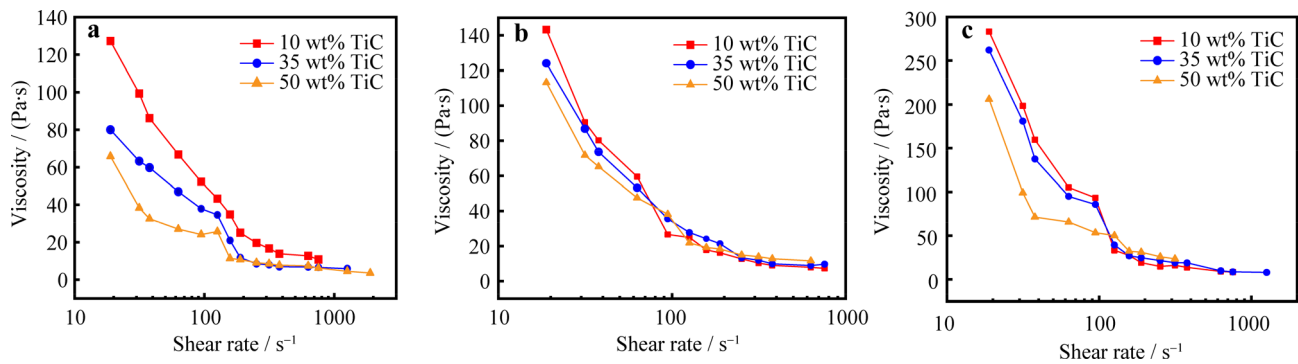


Fig. 4 Rheological properties of epoxy resin–absolute ethanol TiC–316L slurry with different solid contents: **a** 50 vol%, **b** 55 vol% and **c** 60 vol%

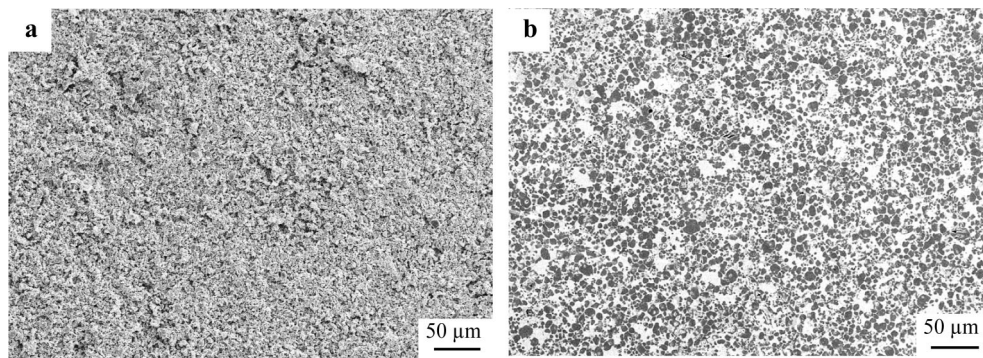


Fig. 5 **a** Fracture SEM image of 35 wt% TiC–316L printed sample and **b** SEM image of 35 wt% TiC–316L sintered sample

polygonal shape and a micrometer grade of particle size which is typically used in the cemented carbide industry. This illustrated that traditional powders used for powder metallurgy could be selected as raw materials in this paper.

3.3 Surface and inner qualities of green samples

Various printing parameters are important factors affecting the surface and internal qualities of green samples. However, the defects of surface and internal qualities caused by the lack of slurry properties, fluidity and curing mode of slurry system cannot be overcome by optimizing printing parameters. The fluidity of the slurry, the proper curing mode and the printing speed are the keys to completely fill the ditches and the gaps between the printing filaments. Through some previous basic studies, the general values of printing parameters are basically determined.

According to the curing mode of epoxy resin–absolute ethanol slurry and its extrusion speed, the printing speed was set at a value of $30 \text{ m}\cdot\text{s}^{-1}$ and the nozzle with a diameter of 0.4 mm was selected to improve the printing efficiency. Under this condition, the influences of layer height on the surface and internal qualities of green samples were studied.

Li et al. [27] studied the surface roughness of samples prepared by the fused deposition modeling (FDM) process.

They concluded that the layer height had a significant influence on surface roughness of the part, because the neck length between adjacent filaments was different with different layer thickness, and it would generate a ditch between two filaments in varying degree. Although with a similar direct writing mode, the slurry in this study has certain flow ability so that curing mode and time of the slurry are also different from that of acrylonitrile butadiene styrene (ABS) or polylactic acid (PLA) used in the FDM process. For the DIW process, the polymerization of the slurry will not be complete within a certain period of time after extrusion, and due to the fluidity, adhesion and elasticity of the slurry, the slurry can flow or deform in a small amount, which leads to a certain degree of filling in the ditches produced between two printing filaments.

According to the phenomenon that occurred during the experiment, the layer height should be slightly smaller than the internal diameter of the nozzle to fill the ditches and gaps between the printing filaments. Therefore, the layer height was set to 0.32, 0.34, 0.36, 0.38 mm, and the roughness of the sample was tested. The surface roughness of the printed samples was hardly affected by the TiC fractions. By taking 35 wt% TiC as an example, the results are shown in Fig. 6. When the layer height was set to 0.32, 0.34, 0.36, 0.38 mm, the surface roughness is 8.933, 7.815, 5.597, 8.338 μm , respectively. Obviously, the roughness of

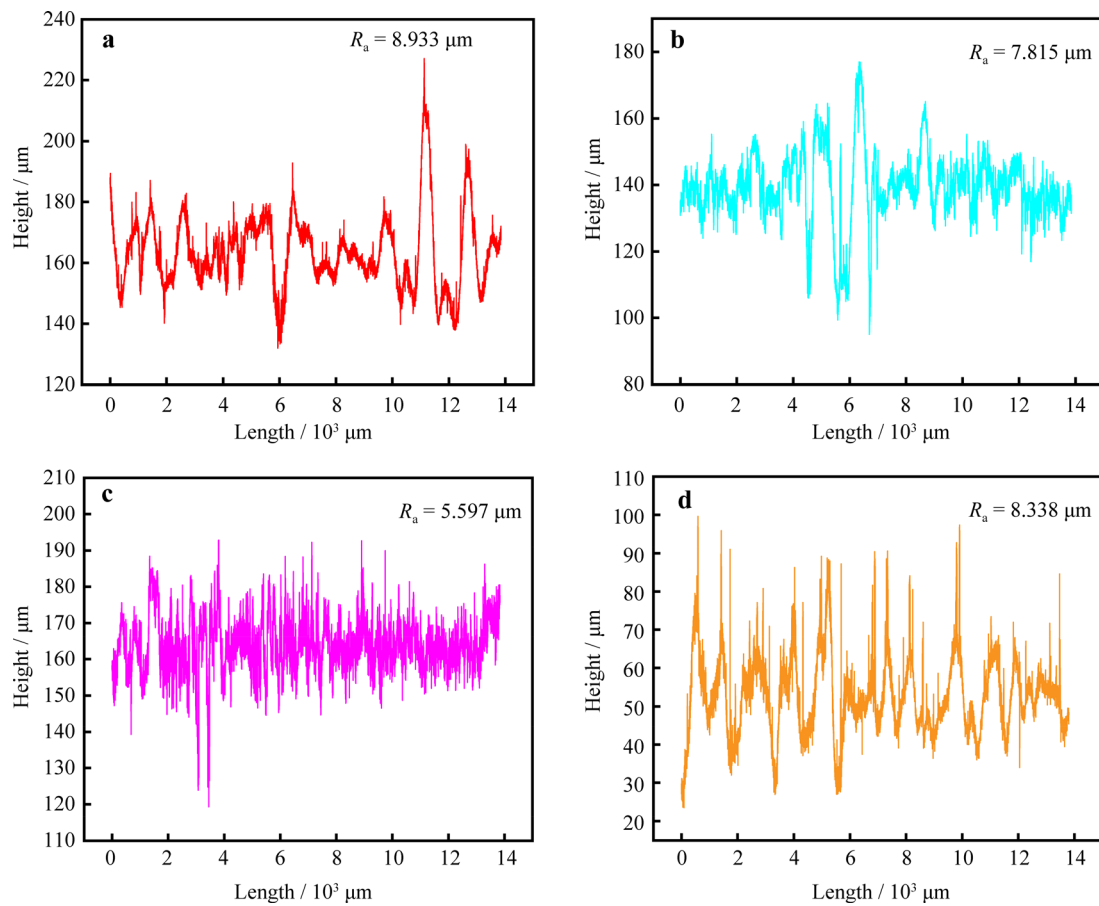


Fig. 6 Surface roughness curves of 35 wt% TiC–316L samples prepared with different layer heights: **a** 0.32 mm, **b** 0.34 mm, **c** 0.36 mm and **d** 0.38 mm

green sample is the best when the layer height is 0.36 mm; the effect of layer height is similar to that of 3D gel-printing of ZrO_2 [28].

When the layer height is 0.38 mm, ditches between two filaments are obvious and can't be filled effectively and regularly. In this case, there are some pores on the surface and inside of the sample and the quality of the sample is bad. When the layer height is 0.41 mm or much larger than the inner diameter of the nozzle, the printing cannot be carried out.

When the layer height is 0.34 mm, the green sample is prone to excessive deformation, and the slurry is easily attached to the nozzle. This destroys the printing filament and has the excessive slurry accumulating in the local position, which results in uneven roughness of the printed body and poor surface quality in the local position. When the layer height is set to 0.32 mm or less, the interval of adjacent printed filaments in the direction of Z-axis is too small to avoid the filaments deformation after they were extruded out the extrusion nozzle. At the same time, a layer

height of less than 0.32 mm leads to excess slurry sticking to the nozzle. The nozzle which is stuck by the slurry breaks the integrity of adjacent printing filaments continuously in the process of moving, which seriously affects the surface and internal qualities in the printing process.

The surface and fracture morphologies of the green sample are shown in Fig. 7. When the layer height is set within the appropriate range, the surface of the green sample has no obvious ridge and valley. The green sample is dense inside and has no obvious defects, and the particle distribution is uniform.

3.4 Properties of sintered samples

Figure 8 shows the samples with 35 wt% TiC before and after sintering. The printed samples containing 10 wt%, 35 wt% and 50 wt% TiC were sintered at 1390, 1450 and 1480 °C, respectively, for 2 h. The relative densities, hardness values and TRS of the samples are shown in Fig. 9. The relative density of sintered samples can reach

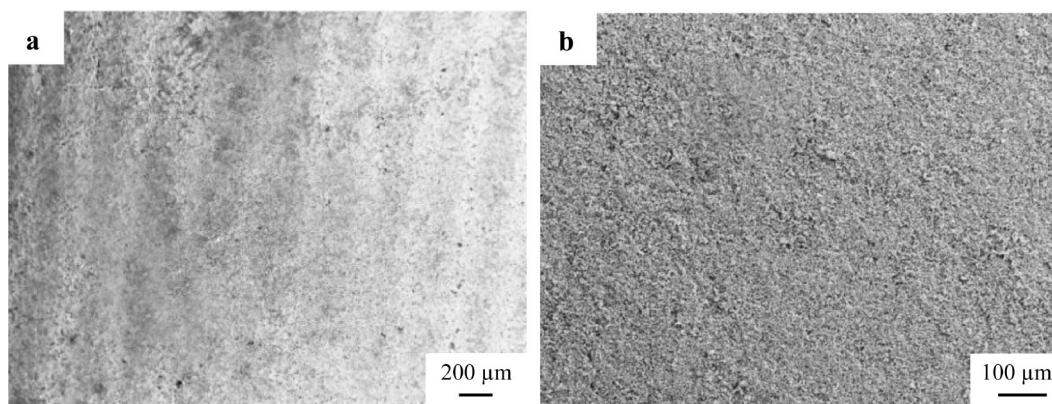


Fig. 7 Surface and internal qualities of 35 wt% TiC-316L green sample prepared with 0.36-mm layer height: **a** surface and **b** internal

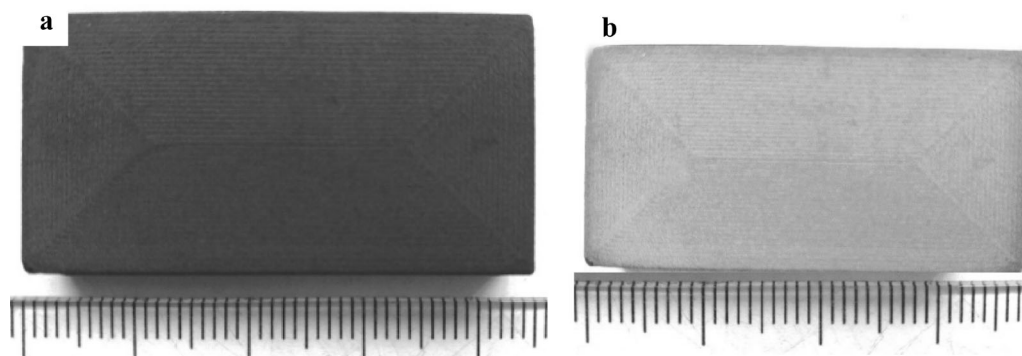


Fig. 8 35 wt% TiC-316L samples: **a** as-printed and **b** as-sintered (viewed from Z-axis direction)

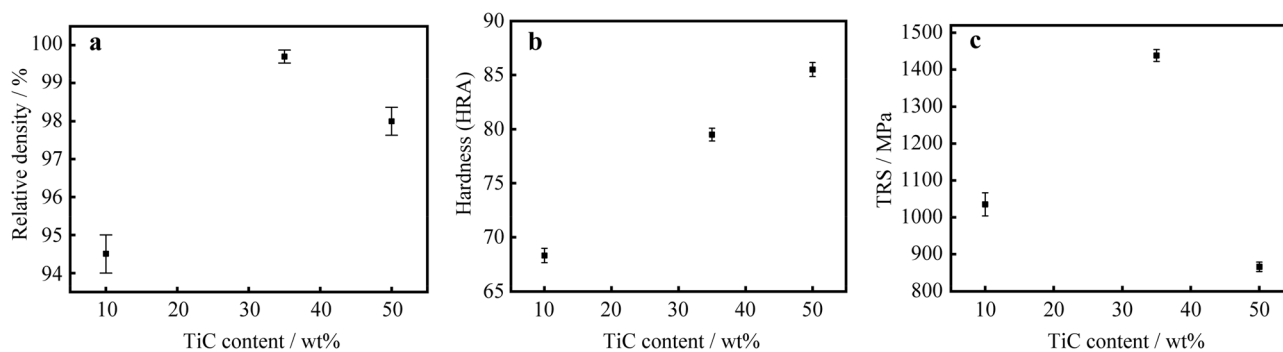


Fig. 9 Properties of sintered samples with different TiC contents prepared by DIW: **a** relative density, **b** hardness and **c** TRS

94.5% (for 10 wt% TiC), 99.3% (for 35 wt% TiC), 98.0% (for 50 wt% TiC). The hardness of sintered samples can reach HRA 68.3 (for 10 wt% TiC), HRA 79.5 (for 35 wt% TiC), HRA 85.5 (for 50 wt% TiC). TRS of sintered samples can reach 1035 MPa (for 10 wt% TiC), 1438 MPa (for 35 wt% TiC), 866 MPa (for 50 wt% TiC).

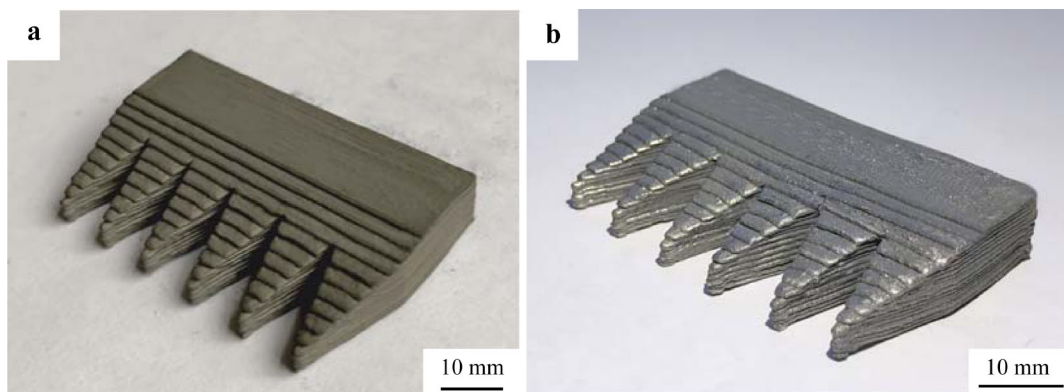
Table 1 shows the properties of TiC-316L MMCs prepared by different processes. As shown in Table 1, the properties of 35 wt% TiC-316L samples prepared by the DIW process with the epoxy resin-absolute ethanol system

are obviously better than that of those prepared with methacrylate-2-hydroxy ethyl (HEMA) system [29].

The samples prepared by the DIW with the epoxy resin-absolute ethanol system have high solid content of printing slurry, good surface roughness, high relative density and high strength. The advantage of 3D printing is the ability to produce products with unique and complex shapes without the help of molds. Figure 10 shows the photographs of 35wt% TiC-316L samples prepared by the DIW with the epoxy resin-absolute ethanol system.

Table 1 Properties of TiC–316L MMCs prepared by different processes

Process	Relative density/%	Hardness (HRA)	TRS/MPa
DIW			
10 wt% TiC–316L	94.5	68.3	1035
35 wt% TiC–316L	99.3	79.5	1438
50 wt% TiC–316L	98.0	85.5	866
3DGP (35 wt% TiC–316L) [22]	97.9	74.9	1230
Ferro-TiC® Grade CM (as-heat treated) ^a	–	86	1276
Conventional powder metallurgy (as-sintered) ^b	99.4	86	1105

^a34 wt% TiC–high chrome tool steel [30]^b50 wt% TiC–high manganese steel [31]**Fig. 10** Photographs of **a** 35 wt% TiC–316L printed and **b** sintered samples prepared by DIW with epoxy resin–absolute ethanol system

3.5 Microstructures and fracture morphologies of sintered samples

The mechanical performances of sintered TiC–316L composite are mainly affected by porosity (relative density), TiC content, TiC particle size and its distribution. For sintered TiC–316L composite, the hardness typically increases and the TRS typically decreases with increasing the TiC content. Furthermore, the higher the relative density is, the higher the composite performances are. Figure 11a–c shows the microstructures of TiC–316L sintered samples with the TiC content of 10 wt%, 35 wt% and 50 wt%, respectively. The black phase is TiC and white phase is stainless steel matrix. It can be seen that TiC particles are uniformly distributed in the stainless steel matrix. It also can be seen that the grain size of TiC particles has no obvious change in comparison with that of the original powder in general, but some grains grow up and some grains grow into an oval shape. The red marks in Fig. 11b, c indicate some oval TiC grains. The fracture morphology of 35 wt% TiC–316L shows brittle fracture characteristics as shown in Fig. 11d. The relative density has effects on the TRS and hardness, and the sample with 35 wt% TiC has the

highest relative density among these three samples so that its hardness and TRS will be improved. The relative density of the sample with 10 wt% TiC has bad effect on its TRS. However, when the TiC content is increased to 50 wt%, the volume proportion of TiC is larger than that of 316L, the TiC particles are susceptible to agglomeration, so the relative density and TRS are reduced, as shown in Fig. 9a–c.

4 Conclusion

In this study, DIW process with an epoxy resin–absolute ethanol system can be successfully used to prepare the TiC–316L MMCs. The maximum solid content of the slurry suitable for DIW is 60 vol% and this is a high level of the solid content for the DIW process, which will be beneficial for enhancing the densification and avoiding the deformation during sintering of the printed samples. In order to take the printing efficiency and printing quality into account in this study, the internal diameter of the nozzle is set to 0.4 mm, the printing speed is set to 30 mm·s^{−1}, and the layer height is set to 0.36 mm.

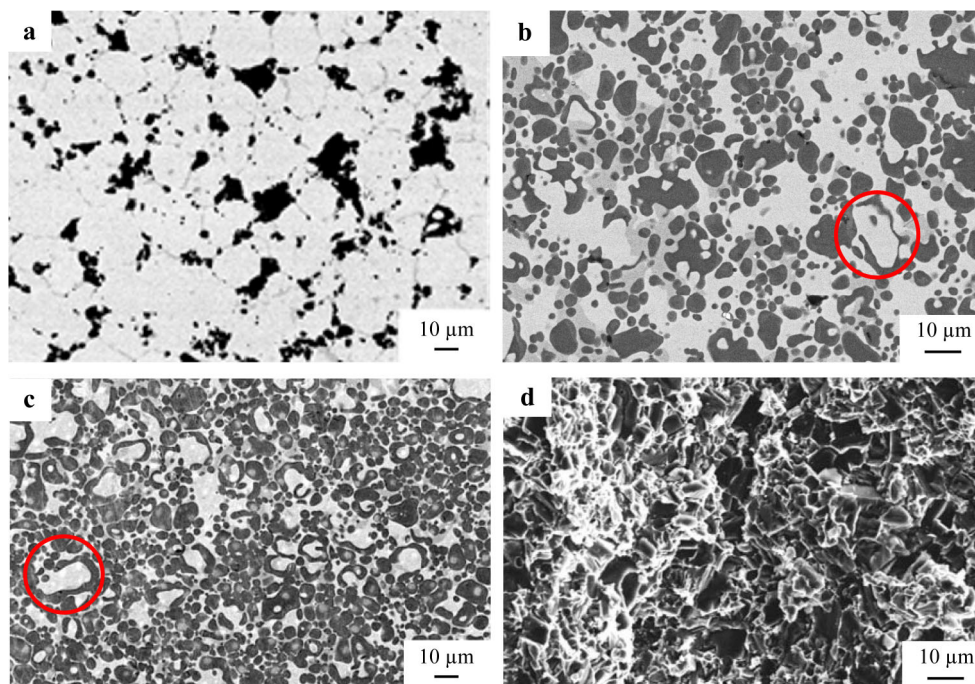


Fig. 11 SEM images of sintered samples: **a** 10 wt% TiC–316L, **b** 35 wt% TiC–316L, **c** 50 wt% TiC–316L and **d** 35 wt% TiC–316L (fracture morphology)

For the sample with 35 wt% TiC–316L, the relative density, hardness and TRS of the sintered sample can reach 99.3%, HRA 79.5 and 1438 MPa, respectively. TiC particles are uniformly distributed in the 316L steel matrix, and the shape of most of the particles is spherical and the shape of a few particles is oval.

Acknowledgements This study was financially supported by Heyuan Science and Technology Project (No. HEKE 000781), the Science and Technology Projects of Guangdong Province (No. 2016B090914001) and Jihua Laboratory Project “Additive Manufacturing for Difficulty-to-Machine Materials” (No. X190061UZ190).

References

- [1] Onuoha CC, Jin CX, Farhat ZN, Kipouros GJ, Plucknett KP. The effects of TiC grain size and steel binder content on the reciprocating wear behaviour of TiC-316L stainless steel cermets. *Wear*. 2016;350–351:116.
- [2] Atik M, Messaddeq SH, Farhat ZN, Aegerter MA, Zarzycki J. Mechanical properties of zirconia-coated 316L austenitic stainless steel. *J Mater Sci Lett*. 1996;15(21):1868.
- [3] Lin S, Xiong WH, Qu J, Yao ZH. Densification and mechanical properties of TiC/316L composites. *J Huazhong Univ Sci Tech*. 2011;38(1):50.
- [4] Wang DF, An XZ, Han P, Jia Q, Fu HT, Zhang H, Yang XH, Zou QC. Multi-particle FEM modelling on hot pressing of TiC-316L composite powders. *Powder Technol*. 2020;361:389.
- [5] Liu SF, Liu DC. Effect of hard phase content on the mechanical properties of TiC-316 L stainless steel cermets. *Int J Refract Met H*. 2019;82:273.
- [6] Jin CX, Onuoha CC, Farhat ZN, Kipouros GJ, Plucknett KP. Reciprocating wear behaviour of TiC-stainless steel cermets. *Tribol Int*. 2017;105:250.
- [7] Jin CX, Onuoha CC, Farhat ZN, Kipouros GJ, Plucknett KP. Microstructural damage following reciprocating wear of TiC-stainless steel cermets. *Tribol Int*. 2017;105:201.
- [8] Fan AP, Xiao PA, Li CK, Xuan CH, Qu XH. Research situation of TiC-based steel bonded carbide. *Powder Metall Tech*. 2013; 31(4):298.
- [9] Lin SJ, Xiong WH. Microstructure and abrasive behaviors of TiC-316L composites prepared by warm compaction and microwave sintering. *Adv Powder Technol*. 2012;23(3):419.
- [10] Hashim L, Looney L. Particle distribution in cast metal matrix composites-Part I. *J Mater Process Technol*. 2002;123(2):251.
- [11] Betts JC, Mordike BL, Grech M. Characterisation, wear and corrosion testing of laser-deposited AISI 316 reinforced with ceramic particles. *Surf Eng*. 2010;26(1–2):21.
- [12] Song B, Dong S, Liao H, Coddet C. Characterisations of TiC particle reinforced FeAl composite part fabricated by selective laser melting. *Mater Res Innov*. 2014;18(1):50.
- [13] Amorim FL, Lohrengel A, Schaefer G, Czelusniak T. A study on the SLS manufacturing and experimenting of TiB₂-CuNi EDM electrodes. *Rapid Prototyping J*. 2013;19(6):418.
- [14] Srinivasa CK, Prabhakar SK, Ramesh CS. Blending of iron and silicon carbide powders for producing metal matrix composites by laser sintering process. *Rapid Prototyping*. 2010;16(4):258.
- [15] Wang XC, Laoui T, Bonse J, Kruth JP, Lauwers B, Froyen L. Direct selective laser sintering of hard metal powders: experimental study and simulation. *Int J Adv Manuf Technol*. 2002; 19(5):351.
- [16] Yao XL, Moon SK, Lee BY, Bi GJ. Effects of heat treatment on microstructures and tensile properties of IN718/TiC nanocomposite fabricated by selective laser melting. *Int J Pr Eng Man-Gt*. 2017;18(12):1693.

- [17] Minas C, Carnelli D, Tervoort E, Studart AR. 3D Printing of emulsions and foams into hierarchical porous ceramics. *Adv Mater*. 2016;28(45):9993.
- [18] Siqueira G, Kokkinis D, Libanori R, Hausmann MK, Gladman AS, Neels A, Tingaut P, Zimmermann T, Lewis JA, Studart AR. Cellulose nanocrystal inks for 3D printing of textured cellular architectures. *Adv Funct Mater*. 2017;27(1604619):1.
- [19] Alison L, Ruehs PA, Studart AR, Sommer MR, Minas C, Tervoort E. 3D printing of concentrated emulsions into multiphase biocompatible soft materials. *Soft Matter*. 2017;13(9):1794.
- [20] Pack RC, Novikov TV, Duty CE, Nlebedim CI, Rios O, Kemp JW, Paranthaman MP, Compton BG. Direct-write 3D printing of NdFeB bonded magnets. *Mater Manuf Process*. 2018;33(1–4):109.
- [21] Ren XY, Shao HP, Lin T, Zheng H. 3D gel-printing-an additive manufacturing method for producing complex shape parts. *Mater Des*. 2016;101(5):80.
- [22] Shao HP, He JZ, Lin T, Zhang ZN, Zhang YM, Liu SW. 3D gel-printing of hydroxyapatite scaffold for bone tissue engineering. *Ceram Int*. 2019;45(1):1163.
- [23] Shao HP, Zhao DC, Lin T, He JZ, Wu J. 3D gel-printing of zirconia ceramic parts. *Ceram Int*. 2017;43(16):13938.
- [24] Papaliangas TT, Anagnostopoulos CA. Experimental investigation of epoxy resin and sand mixes. *J Geotech Geoenviron*. 2012;138(7):841.
- [25] Lutz, Kindersberger J. Influence of absorbed water on volume resistivity of epoxy resin insulators. In: IEEE International Conference on Solid Dielectrics. Potsdam, Germany. 2010.643.
- [26] Wang HB, Wei XP, He YX, Li HS. Investigation of thermal decomposition kinetics of epoxy resin cured by polyamide. *Chinese J Colloid Polym*. 2011;29(2):75.
- [27] Li HB, Wang TY, Sun J, Yu ZQ. The adaptive slicing algorithm and its impact on the mechanical property and surface roughness of freeform extrusion parts. *Virtual Phys Prototy*. 2016;11(1):27.
- [28] Zhang ZZ, Lin T, Shao HP, Zhang YM, Wang LH, Deng X. Preparation of 3DGP dense zirconia parts by two-step method: staggered stacking method and printing wire deformation. *Ceram Int*. 2020;46(5):6491.
- [29] Ji ZH, Zhao DC, Hao JJ, Zhang XD, Wang JZ. 3D gel-printing of TiC-reinforced 316L stainless steel: influence of the printing parameters. *J Mater Eng Perform*. 2018;27(10):5500.
- [30] Lin T, Guo Y, Wang Z, Shao HP, Lu HY, Li FH, He XB. Effects of chromium and carbon content on microstructure and properties of TiC-steel composites. *Int J Refract Met H*. 2018;72:228.
- [31] Wang Z, Lin T, He XB, Shao HP, Zheng JS, Qu XH. Microstructure and properties of TiC-high manganese steel cermet prepared by different sintering processes. *J Alloy Compd*. 2015;650:918.